Volume 10 | Number 45 | 7 December 2019 | Pages 10449–10656

Chemical Science

rsc.li/chemical-science

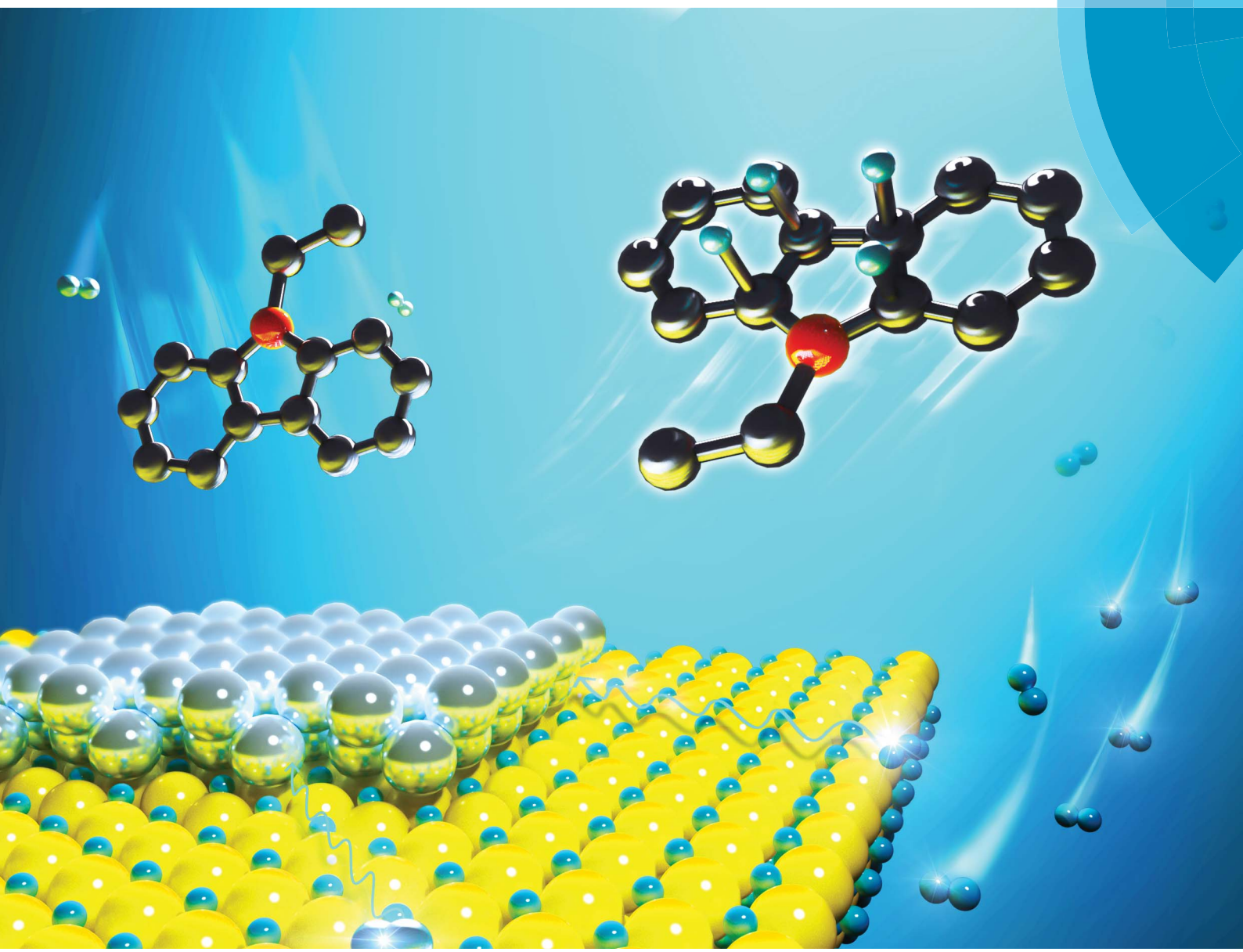

ISSN 2041-6539

ROYAL SOCIETY OF CHEMISTRY | Celebrating IYPT 2019

EDGE ARTICLE

Jie Zheng, Xingguo Li *et al.*

A rare earth hydride supported ruthenium catalyst for the hydrogenation of *N*-heterocycles: boosting the activity *via* a new hydrogen transfer path and controlling the stereoselectivity

Chemical Science

EDGE ARTICLE

View Article Online
View Journal | View Issue

Cite this: *Chem. Sci.*, 2019, **10**, 10459

All publication charges for this article have been paid for by the Royal Society of Chemistry

A rare earth hydride supported ruthenium catalyst for the hydrogenation of *N*-heterocycles: boosting the activity *via* a new hydrogen transfer path and controlling the stereoselectivity†

Yong Wu,[a] Hongen Yu,[a] Yanru Guo,[a] Xiaojing Jiang,[a] Yue Qi,[a] Bingxue Sun,[a] Haiwen Li,[b] Jie Zheng *[a] and Xingguo Li *[a]

Received 30th August 2019
Accepted 10th October 2019

DOI: 10.1039/c9sc04365a

rsc.li/chemical-science

Hydrogenation of *N*-heterocycles is of great significance for their wide range of applications such as building blocks in drug and agrochemical syntheses and liquid organic hydrogen carriers (LOHCs). Pursuing a better hydrogenation performance and stereoselectivity, we successfully developed a rare earth hydride supported ruthenium catalyst Ru/YH_3 for the hydrogenation of *N*-heterocycles, especially *N*-ethylcarbazole (NEC), the most promising LOHC. Full hydrogenation of NEC on Ru/YH_3 can be achieved at 363 K and 1 MPa hydrogen pressure, which is currently the lowest compared to previous reported catalysts. Furthermore, Ru/YH_3 shows the highest turnover number, namely the highest catalytic activity among the existing catalysts for hydrogenation of NEC. Most importantly, Ru/YH_3 shows remarkable stereoselectivity for all-*cis* products, which is very favorable for the subsequent dehydrogenation. The excellent performance of Ru/YH_3 originates from the new hydrogen transfer path from H_2 to NEC *via* YH_3. Ru/LaH_3 and Ru/GdH_3 also reveal good activity for hydrogenation of NEC and Ru/YH_3 also possesses good activity for hydrogenation of 2-methylindole, indicating that the use of rare earth hydride supported catalysts is a highly effective strategy for developing better hydrogenation catalysts for *N*-heterocycles.

Introduction

N-Heterocycles have been attracting much attention because of their great versatility in many pharmaceuticals, alkaloids, agrochemicals, and fine chemicals.[1–4] Recently, liquid organic hydrogen carriers (LOHCs) have been proposed as convenient and safe candidates for hydrogen storage and *N*-heterocycles are very typical LOHCs for their high hydrogen capacities and relatively low operating temperatures.[5–8] One of the most well-studied LOHCs is *N*-ethylcarbazole (NEC), whose hydrogen-rich state dodecahydro-*N*-ethylcarbazole (12H-NEC) is liquid at room temperature with a hydrogen capacity of 5.8 wt%. Additionally, the operating temperature for hydrogen storage on NEC is below 473 K for the hydrogenation enthalpy is only −50.6 kJ (mol^{-1} H_2).[9–13]

The kinetics of hydrogenation of *N*-heterocycles is usually sluggish, which is an obstacle for their application as LOHCs. Consequently, effective hydrogenation catalysts are urgently needed. Many homogenous or heterogeneous catalysts were developed for hydrogenation of *N*-heterocycles, which are mainly quinoline and its derivatives.[3,14–21] For the hydrogenation of NEC, the catalysts are mainly Ru based heterogeneous catalysts.[22–26] Many factors such as supports and particle sizes will influence the catalytic performance, since the hydrogenation reaction is a stepwise complex reaction (Fig. 1).

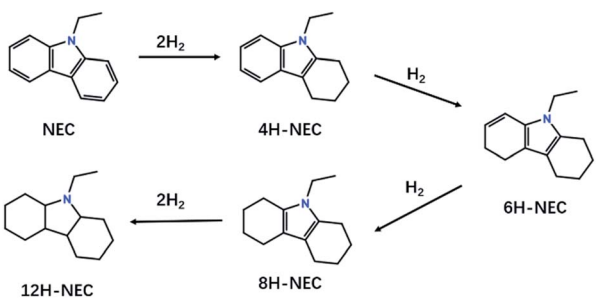

Fig. 1 Reaction process of the hydrogenation of NEC.

[a]*Beijing National Laboratory for Molecular Science (BNLMS), College of Chemistry and Molecular Engineering, Peking University, Beijing 100871, China*

[b]*Platform of Inter/Transdisciplinary Energy Research (Q-PIT), International Research Center for Hydrogen Energy, International Institute for Carbon-Neutral Energy Research (I2CNER), Kyushu University, 744 Motooka Nishi-ku, Fukuoka 819-0395, Japan. E-mail: xgli@pku.edu.cn; Fax: +86-10-62765930; Tel: +86-10-62765930*

† Electronic supplementary information (ESI) available: Experimental details and additional figures. See DOI: 10.1039/c9sc04365a

Recently, we demonstrated that reversible hydrogen absorption/desorption, the very fundamental property of metal hydrides, can be used to promote the hydrogenation of NEC. The Ni/Al_2O_3-YH_3 catalyst we developed is the most efficient noble metal free catalyst for NEC hydrogenation and its catalytic activity is close to that of Ru/Al_2O_3, the state-of-the-art catalyst for the hydrogenation of NEC.[27,28] To further increase catalytic activity and decrease the dosage of the precious metal Ru, we considered that we can directly use YH_3 as a support material. Some rare earth hydrides are used as support materials of Ru catalysts for ammonia synthesis.[29] Although the original activity of the obtained catalysts is promising, the stability is a problem due to the formation of rare earth nitrides.[29] However, this problem will not occur in the hydrogenation of *N*-heterocycles since there is no nitrogen.

Here we report a robust Ru/YH_3 catalyst for the hydrogenation of *N*-heterocycles. The temperature for complete NEC hydrogenation on Ru/YH_3 can be as low as 363 K. For sufficient reaction rate, we choose 403 K as the optimized temperature. At 403 K, the hydrogen pressure can be below 1 MPa. Besides the lowest hydrogenation temperature and hydrogen pressure among the reported studies, the hydrogenation rate is also the fastest while using the same amount of Ru. Additionally, Ru/YH_3 exhibits extraordinary stereoselectivity for the all-*cis* products.

Based on our experimental results, we believe that there is a new hydrogen transport path in our system during the reaction, which contributes to the high catalytic activity. More specifically, there is hydrogen transfer between gaseous hydrogen and hydrogen in YH_3 as YH_3 is also a hydrogen storage material which can absorb and desorb hydrogen reversibly rapidly, so that the hydrogen in YH_3 can spill-over to Ru, enabling the hydrogenation of NEC molecules absorbed on Ru.

Results and discussion

The properties of catalysts

Ru/YH_3 was obtained by an improved chemical vapor deposition method and Ru/Al_2O_3 was prepared by the same method.[29–31] Ru/Al_2O_3 is a reference catalyst. Fig. 2 shows the XRD patterns of Ru/YH_3 and Ru/Al_2O_3. There are only signals of crystalline YH_3 (ICSD 98-015-4809)[32] in the XRD patterns of Ru/YH_3. The XRD patterns of Ru/Al_2O_3 are almost the same as the XRD patterns of pristine Al_2O_3 (ICSD 98-008-8027)[33] (Fig. S1†). The signal peaks of Al_2O_3 are broad, as the size is about 20 nm according to the supplier. There are no signals of Ru in the XRD patterns, indicating that the size of Ru is very small.

The TEM images of YH_3 and Al_2O_3 (Fig. S2†) and the HRTEM images of Ru/YH_3 and Ru/Al_2O_3 (Fig. 3) well prove the point. The size of YH_3 ranges from 50 nm to 500 nm, while the size of Al_2O_3 is around 20 nm as expected. The size of Ru is approximately 5 nm, and Ru nanoparticles are uniformly dispersed on the supports according to the elemental mapping for both Ru/YH_3 and Ru/Al_2O_3. The lattice fringes of Ru (010), Ru (002), Ru (011) and YH_3 (111) can be seen in the HRTEM images of Ru/YH_3, implying that YH_3 has not been oxidized during the catalyst preparation process, which corresponds with the results of XRD patterns of Ru/YH_3.

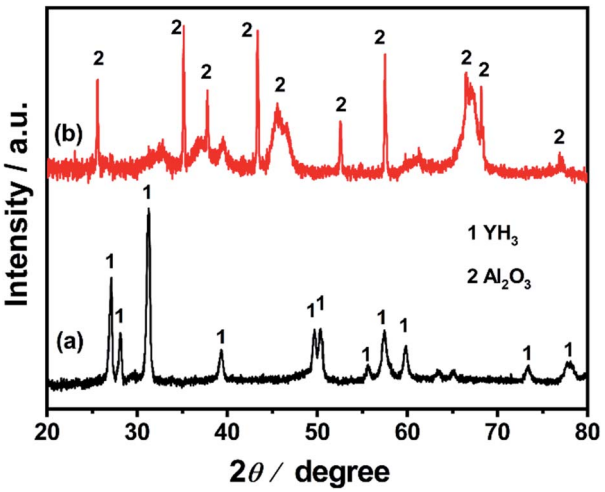

Fig. 2 XRD patterns of (a) Ru/YH_3 and (b) Ru/Al_2O_3.

This can also be demonstrated from the XPS spectra of Ru/YH_3 (Fig. S3†). The binding energies that can be ascribed to Y $3d_{5/2}$ and Y $3d_{3/2}$ are 157.8 eV and 159.8 eV, while the previously reported results for YH_3 are 157.7 eV and 159.6 eV.[34,35] In the case of Y_2O_3, they are 156.8 eV and 158.9 eV. In the case of YH_2, they are 156.5 eV and 158.5 eV.[34,35] These results indicate that there is no surface oxidation in Ru/YH_3. The binding energy of Ru $3d_{5/2}$ appears at 280.4 eV, exhibiting a positive chemical shift of *ca.* 0.4 eV from the nominal value of 280.0 eV in Ru nanoparticles.[36] However, the binding energy of Ru $3d_{5/2}$ in Ru/Al_2O_3 appears at the same position as that in Ru/YH_3, indicating the same electronic effect of support materials on Ru/Al_2O_3 and Ru/YH_3.

Since the particle sizes of YH_3 and Al_2O_3 are much different and Al_2O_3 is porous, the surface areas of Ru/YH_3 and Ru/Al_2O_3 must be different. Indeed, the BET surface areas of Ru/YH_3 and Ru/Al_2O_3 are 11.3 and 103.2 $m^2\ g^{-1}$ from the nitrogen adsorption/desorption isotherms (Fig. S4†), respectively. Due to the bigger surface area of Ru/Al_2O_3, which signifies a smaller loss of Ru during the chemical vapor deposition process, the Ru loading amount of Ru/Al_2O_3 is 4.6 wt% while that of Ru/YH_3 is 1.3 wt% based on the results of ICP-OES, even though the expected loading amounts are 5 wt% for all catalysts.

The catalytic performances

It seems that the catalytic performance of Ru/YH_3 will be terrible because of the low surface area and low Ru loading amount. Unexpectedly, the hydrogenation rates are almost the same when adding the same amount of Ru/YH_3 and Ru/Al_2O_3 (Fig. 4a). The ^1H NMR spectra of the corresponding hydrogenation products (Fig. 4b) confirm that the products are both complete hydrogenated products (12H-NEC) as the chemical shifts (>3.6 ppm) ascribed to H which bonds to C (sp^2) disappear.[9]

As the Ru loading amount of Ru/Al_2O_3 is higher than that of Ru/YH_3, the TON (turnover number, the amount of substance transformed per mole active metal per hour) of Ru/YH_3 is higher than the TON of Ru/Al_2O_3 (Table 1). That is, the catalytic

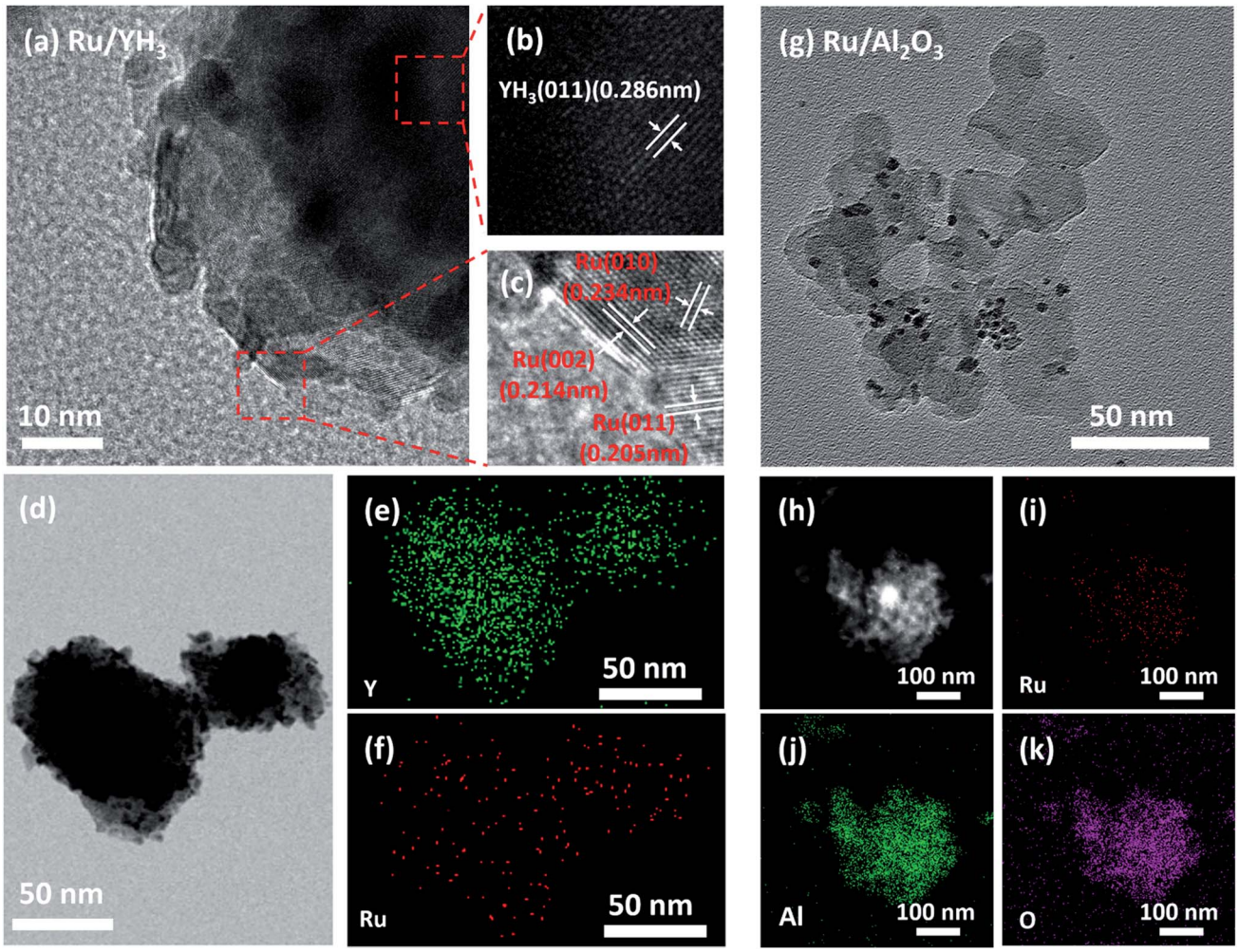

Fig. 3 HRTEM images and elemental mapping of (a–f) Ru/YH_3 and (g–k) Ru/Al_2O_3.

performance of Ru/YH_3 is better. Compared to the previously reported catalysts for NEC hydrogenation, the TON of Ru/YH_3 is also the highest (Table 1).

Additionally, the hydrogenation on the Ru/YH_3 catalyst is stereoselective. There are six stereoisomers in full hydrogenation products of NEC.[9] When the catalyst is Ru/Al_2O_3, the products are (4a S, 4b R, 8a S, 9a S)–12H-NEC (47 mol%), (4a S, 4b R, 8a R, 9a S)–12H-NEC (41 mol%) and (4a S, 4b S, 8a R, 9a S)–12H-NEC (12 mol%) (Fig. 4b), which is in agreement with the previous reports.[9] When the catalyst is Ru/YH_3, the products are (4a S, 4b R, 8a R, 9a S)–12H-NEC (91 mol%) and (4a S, 4b S, 8a R, 9a S)–12H-NEC (9 mol%) (Fig. 4b). The main product on the Ru/YH_3 catalyst is an all-*cis* product, which is easier to dehydrogenate on the catalytic surface with less steric hindrance. The formation all-*cis* 12H-NEC is favourable in dynamics but unfavourable in thermodynamics; therefore faster rates may result in a better stereoselectivity. Stereoselective hydrogenation of NEC was only reported on Ru black before; however only 70 mol% all-*cis* 12H-NEC was obtained.[22,23] The authors proved that the stereoselectivity originated from the flatter surface of Ru black, which is unfavourable for stereoisomerization from all-*cis* 12H-NEC to other more thermodynamically stable products.[22,23]

The surface structure of Ru in Ru/YH_3 is similar to that of Ru black according to the HRTEM images (Fig. 3a–c), resulting from the low surface area of YH_3. However, the hydrogenation rate on Ru/YH_3 is much faster than that on Ru black; hence Ru/YH_3 exhibits a better stereoselectivity for all-*cis* 12H-NEC.

To further investigate the influences of temperature and hydrogen pressure, we performed a series of experiments under different conditions. The results (Fig. 4c and d) show that full hydrogenation can be accomplished at only 363 K (Fig. S5†). The higher the temperature, the faster the reaction rate. However, the increase is unremarkable when the temperature is over 403 K, which is limited by mass transfer of substrates.[9] As a result, we choose 403 K as the optimized temperature. An increment of the reaction rate is also observed with increased hydrogen pressure. When the pressure is 3 MPa, the time to full hydrogenation is as long as 60 h (Fig. S6†). Therefore, high pressure is necessary to obtain a high enough rate in this case.

The H transfer mechanism

The catalytic activity of Ru/YH_3 is superior to that of Ru/Al_2O_3, while the surface area of Ru/YH_3 is much smaller than the surface area of Ru/Al_2O_3. The XPS spectra of Ru/Al_2O_3 and Ru/

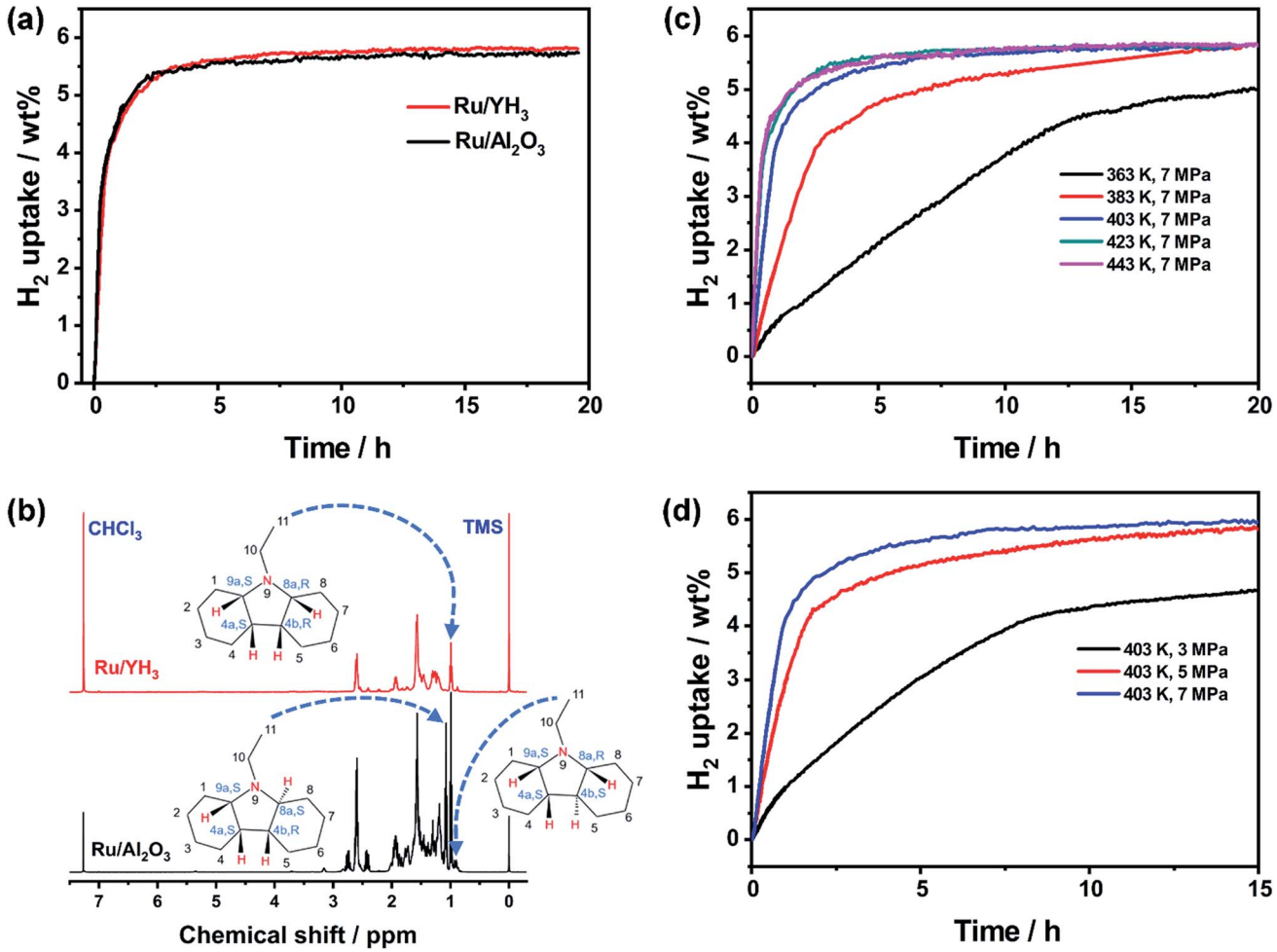

Fig. 4 (a) Hydrogen absorption kinetics and (b) ^{1}H NMR spectra of corresponding hydrogenation products of NEC using Ru/YH_3 and Ru/Al_2O_3 as catalysts (403 K, 7 MPa H_2, 1.00 g NEC, 50 mg catalysts). Hydrogen absorption kinetics of NEC using Ru/YH_3 as the catalyst (c) at different temperatures and (d) under different hydrogen pressures (1.00 g NEC, 50 mg catalyst).

YH_3 indicate that the electron effect of Al_2O_3 and YH_3 is the same (Fig. S4†). The size of Ru is similar in the two catalysts and the flat surface of Ru in Ru/YH_3 is unhelpful to surpass Ru/Al_2O_3. As YH_3 has no activity (Fig. S7†), it must have some other positive influence on the catalytic hydrogenation of NEC.

Although rare earth hydrides can reversibly adsorb and desorb hydrogen, they are not good hydrogen storage materials

Table 1 The catalytic performances of different catalysts for the hydrogenation of NEC

Catalyst	Condition	Yield/%	TON[a]/h^{-1}	Reference
5 wt% Ru/Al_2O_3	5 wt% Cat., 403 K, 7 $MPaH_2$	99.5	68.7	9
5 wt% Ru/TiO_2	5 wt% Cat., 403 K, 7 $MPaH_2$	95.0	17.8	24
Ru black	5 wt% Cat., 403 K, 7 $MPaH_2$	85.0	0.5	24
5 wt% Ru/AC	10 wt% Cat., 403 K, 7 $MPaH_2$	100	23.2	22
5 wt% Rh/AC	20 wt% Cat., 403 K, 7 $MPaH_2$	100	17.0	22
5 wt% Pd/AC	20 wt% Cat., 403 K, 7 $MPaH_2$	67.0	7.7	22
F–$LaNi_5$	10 wt% Cat., 443 K, 6 $MPaH_2$	87.9	0.5	37
RANEY® Ni	10 wt% Cat., 453 K, 5 $MPaH_2$	86.2	0.4	38
65 wt% Ni/Al_2O_3–SiO_2	20 wt% Cat., 403 K, 7 $MPaH_2$	50.0	0.3	23
5.2 wt% Ru/Al_2O_3	10 wt% Cat., 413 K, 6 $MPaH_2$	96.6	24.2	28
0.52 mol% Pd_2Ru/SiCN	20 wt% Cat., 383 K, 2 $MPaH_2$	97.9	7.2	39
4.6 wt% Ru/Al_2O_3	5 wt% Cat., 403 K, 7 $MPaH_2$	100	90.0	This work
1.3 wt% Ru/YH_3	5 wt% Cat., 403 K, 7 $MPaH_2$	100	318.6	This work

[a] TON is calculated as the amount of substance completely transformed per mole active metal per hour based on the hydrogenation curves.

due to their low hydrogen capacities and high dehydrogenation temperatures. However, this property may be helpful in other application domains.[27,40,41] The conversion temperature between YH_3 and YH_2 is as high as 642 K at 101 325 Pa hydrogen pressure.[42] In spite of this, some hydrogen can be released under the conditions of hydrogenation reaction according to the pressure-composition isotherm (PCI) curves of Y–H systems.[42] In order to illustrate this, the TPD/MS curves of YH_3 and Ru/YH_3 are measured. The onset hydrogenation temperatures are around 373 K for both YH_3 and Ru/YH_3 (Fig. S8a†), suggesting that YH_3 can desorb some hydrogen during the hydrogenation reaction. In contrast, the transformation of YH_{3-x} into YH_3 is easy at the hydrogenation temperature of NEC according to the PCI curve of YH_3.[42] In this situation, the hydrogenation of NEC on the Ru/YH_3 catalyst can be schematically described as in eqn (1) and (2):

$$YH_3 + \text{NEC-Ru} \rightarrow YH_{3-x} + \text{12H-NEC-Ru} \quad (1)$$

$$YH_{3-x} + H_2 \rightarrow YH_3 \quad (2)$$

Here YH_{3-x} $(0 < x < 1)$ denotes partially H deficient YH_3. NEC-Ru and 12H-NEC-Ru mean NEC and 12H-NEC molecules adsorbed on the Ru surface. We have stated that eqn (1) and (2) are thermodynamically feasible by introducing the concept of hydrogen chemical potential in our previous report.[27]

To verify the assumption experimentally, we conduct the hydrogenation reaction using stoichiometric Ru/YH_3 without H_2. To avoid the influence of the gaseous H_2 from the pyrolysis of YH_3, we first set the temperature as 353 K, which is lower than the onset decomposition temperature of YH_3. The NMR spectra of the product (Fig. S8b†) clearly show that a partial hydrogenation product tetrahydro-*N*-ethylcarbazole (4H-NEC) is obtained, and the pressure does not increase during the reaction. When the temperature is up to 403 K, the result (Fig. S8b†) is similar except that the amount of 4H-NEC increases. Although YH_3 can release H_2 at 403 K, the rate is very slow (Fig. S6†), consequently the pressure still does not increase. These results illustrate that there is indeed a new hydrogen transfer path in the hydrogenation reaction as eqn (1) and (2) show, which is the main cause of the high activity of Ru/YH_3.

More general applicability

Although the catalytic performance of Ru/YH_3 is excellent, the hydrogen pressure is very high to guarantee the selectivity for full hydrogenation products, which is unfavourable for the practical application. The plateau pressure of YH_3 is lower than 1.4 kPa when the temperature is lower than 523 K, indicating that the reversible hydrogen absorption and desorption of YH_3 can occur under much lower hydrogen pressure at reaction temperature.[42] As the new hydrogen transfer path plays a key role in the reaction, the hydrogen pressure may be decreased by using more Ru/YH_3 catalyst.

To test the hypothesis, we use 100 wt% catalyst and 1 MPa H_2 to run the hydrogenation reaction. Indeed, the hydrogenation rate is still fast, especially in the initial stage (Fig. 5a) when using Ru/YH_3. Oppositely, the performance of Ru/Al_2O_3 is

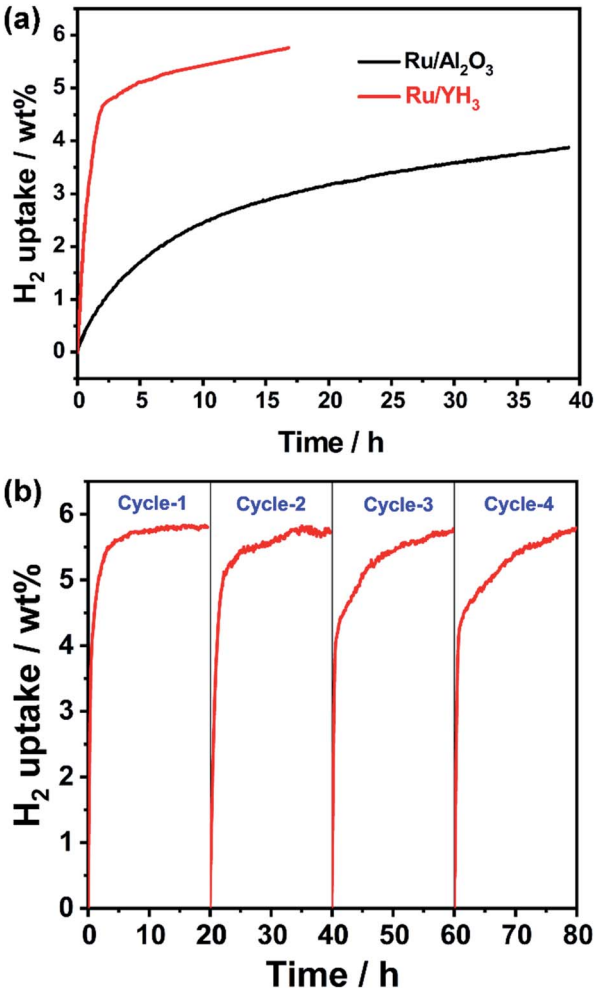

Fig. 5 (a) Hydrogen absorption kinetics of NEC using Ru/YH_3 and Ru/Al_2O_3 as catalysts (403 K, 1 MPa H_2, 1.00 g NEC, 1.00 g catalyst); (b) hydrogenation kinetics on Ru/YH_3 for four repeated cycles (403 K, 7 MPa H_2, 1.00 g NEC per experiment, 50 mg catalyst).

undesirable under this condition (Fig. 5a). If we use a flow reactor and maintain the hydrogen pressure, which is closer to the practical situation in industrial production, the ratio of Ru/YH_3 to NEC will be higher and the reaction rate will be faster.

If we want to use Ru/YH_3 in a continuous flow reactor, the catalytic stability is significant. The results of stability test (Fig. 5b) show that the rates are relatively stable, while the slight decrease of rates can be attributed to the unseparated products. In other words, the stability of the Ru/YH_3 catalyst is satisfactory.

To investigate the range of applicability, we use Ru/YH_3 to catalyse the hydrogenation reactions of another *N*-heterocycle, 2-methylindole (MID), under similar conditions. The results (Fig. 6a and S9†) show that MID can be hydrogenated completely in 10 h, implying that Ru/YH_3 is a versatile catalyst for hydrogenation of *N*-heterocycles to some extent.

Considering the fact that the properties of rare earth hydrides are similar, we use LaH_3 and GdH_3 to replace YH_3 in our experiments. As expected, the hydrogenation reaction can

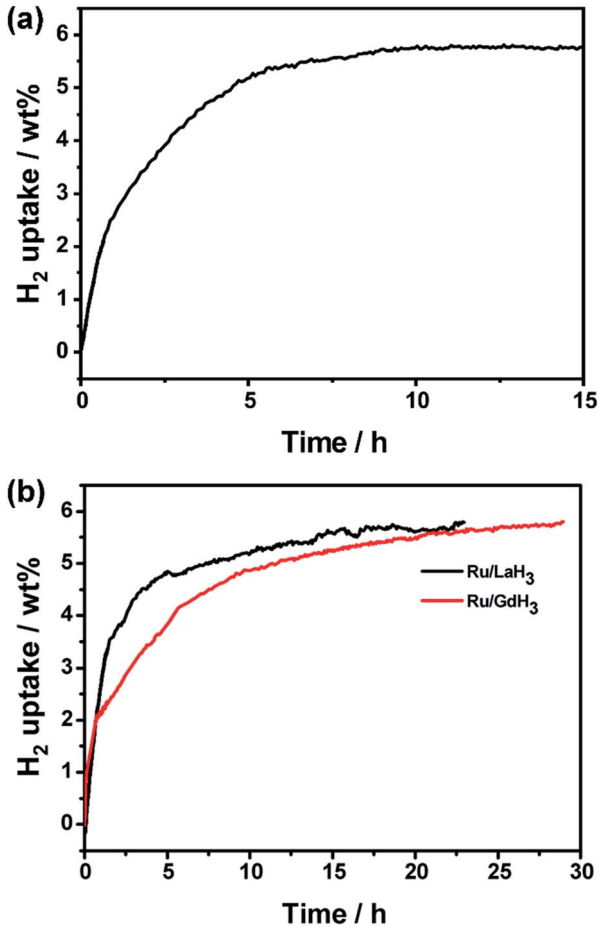

Fig. 6 (a) Hydrogen absorption kinetics of 2-methylindole using Ru/YH_3 as the catalyst; (b) hydrogen absorption kinetics of NEC using Ru/LaH_3 and Ru/GdH_3 as the catalyst. (403 K, 7 MPa H_2, 1.00 g substrates, 50 mg catalyst).

also be completed with high activity (Fig. 6b). This implies that rare earth hydrides are generic in this system. The overall rate of Ru/LaH_3 is faster than that of Ru/GaH_3, but slower than that of Ru/YH_3. As the density becomes higher from Y to La to Gd, the volume and the surface area will be smaller when the weight is the same. Thus, the amount of Ru loading will decrease, resulting in worse catalytic performance. As a consequence, YH_3 is a better choice for this system.

Conclusions

In summary, we have developed a rare earth hydride supported ruthenium catalyst Ru/YH_3 for hydrogenation of *N*-heterocycles. For hydrogenation of a well-studied and promising liquid organic hydrogen carrier, ethylcarbazole (NEC), Ru/YH_3 shows the highest catalytic activity as it has the highest turnover number. This means that the amount of precious metal Ru can be decreased, which is essential for the application in hydrogen storage. The outstanding activity is due to the new hydrogen transfer path from H_2 to NEC provided by reversible hydrogen absorption and desorption of YH_3. Additionally, complete hydrogen adsorption can be accomplished at the lowest temperature (363 K) and the lowest hydrogen pressure (1 MPa). Moreover, Ru/YH_3 is also robust in terms of stability, low-pressure hydrogenation and stereoselectivity for all-*cis* products, which is desirable from the point of view of the application of NEC in hydrogen storage. The Ru/YH_3 catalyst is also active for hydrogenation of 2-methylindole, another *N*-heterocycle. Other rare earth hydrides are also effective supports. The idea of rare earth hydride supported catalysts is an excellent strategy for developing *N*-heterocycle hydrogenation catalysts and new applications of rare earth hydrides.

Conflicts of interest

There are no conflicts to declare.

Acknowledgements

The authors acknowledge the MOST of China (No. 2018YFB1502102) and NSFC (No. 51771002, 51431001, 21771006, U1607126 and 21621061). The authors are also grateful for support from the Progress 100 program of Kyushu University.

Notes and references

1 V. Sridharan, P. A. Suryavanshi and J. Carlos Menendez, *Chem. Rev.*, 2011, **111**, 7157–7259.
2 J. D. Scott and R. M. Williams, *Chem. Rev.*, 2002, **102**, 1669–1730.
3 Y. Wu, Z. Chen, W.-C. Cheong, C. Zhang, L. Zheng, W. Yan, R. Yu, C. Chen and Y. Li, *Chem. Sci.*, 2019, **10**, 5345–5352.
4 P. Ryabchuk, A. Agapova, C. Kreyenschulte, H. Lund, H. Junge, K. Junge and M. Beller, *Chem. Commun.*, 2019, **55**, 4969–4972.
5 R. H. Crabtree, *Energy Environ. Sci.*, 2008, **1**, 134–138.
6 T. He, Q. Pei and P. Chen, *J. Energy Chem.*, 2015, **24**, 587–594.
7 P. M. Modisha, C. N. M. Ouma, R. Garidzirai, P. Wasserscheid and D. Bessarabov, *Energy Fuels*, 2019, **33**, 2778–2796.
8 M. Niermann, A. Beckendorff, M. Kaltschmitt and K. Bonhoff, *Int. J. Hydrogen Energy*, 2019, **44**, 6631–6654.
9 K. M. Eblagon, D. Rentsch, O. Friedrichs, A. Remhof, A. Zuettel, A. J. Ramirez-Cuesta and S. C. Tsang, *Int. J. Hydrogen Energy*, 2010, **35**, 11609–11621.
10 M. Sobota, I. Nikiforidis, M. Amende, B. S. Zanon, T. Staudt, O. Hoefert, Y. Lykhach, C. Papp, W. Hieringer, M. Laurin, D. Assenbaum, P. Wasserscheid, H.-P. Steinrueck, A. Goerling and J. Libuda, *Chem.–Eur. J.*, 2011, **17**, 11542–11552.
11 Y. Dong, M. Yang, P. Mei, C. Li and L. Li, *Int. J. Hydrogen Energy*, 2016, **41**, 8498–8505.
12 B. Wang, T.-y. Chang, Z. Jiang, J.-j. Wei, Y.-h. Zhang, S. Yang and T. Fang, *Int. J. Hydrogen Energy*, 2018, **43**, 7317–7325.
13 B. Wang, T.-y. Chang, X. Gong, Z. Jiang, S. Yang, Y.-s. Chen and T. Fang, *ACS Sustainable Chem. Eng.*, 2019, **7**, 1760–1768.

14 I. Sorribes, L. Liu, A. Domenech-Carbo and A. Corma, *ACS Catal.*, 2018, **8**, 4545–4557.
15 A. Vivancos, M. Beller and M. Albrecht, *ACS Catal.*, 2018, **8**, 17–21.
16 X. Xue, M. Zeng and Y. Wang, *Appl. Catal., A*, 2018, **560**, 37–41.
17 J.-W. Zhang, D.-D. Li, G.-P. Lu, T. Deng and C. Cai, *ChemCatChem*, 2018, **10**, 4980–4986.
18 S. Zhang, Z. Xia, T. Ni, Z. Zhang, Y. Ma and Y. Qu, *J. Catal.*, 2018, **359**, 101–111.
19 G. Jaiswal, M. Subaramanian, M. K. Sahoo and E. Balaraman, *ChemCatChem*, 2019, **11**, 2449–2457.
20 S. Wang, H. Huang, C. Bruneau and C. Fischmeister, *ChemSusChem*, 2019, **12**, 2350–2354.
21 Z. Wei, F. Shao and J. Wang, *Chin. J. Catal.*, 2019, **40**, 980–1002.
22 K. M. Eblagon, K. Tam and S. C. E. Tsang, *Energy Environ. Sci.*, 2012, **5**, 8621–8630.
23 K. M. Eblagon, K. Tam, K. M. K. Yu and S. C. E. Tsang, *J. Phys. Chem. C*, 2012, **116**, 7421–7429.
24 K. M. Eblagon, K. Tam, K. M. K. Yu, S.-L. Zhao, X.-Q. Gong, H. He, L. Ye, L.-C. Wang, A. J. Ramirez-Cuesta and S. C. Tsang, *J. Phys. Chem. C*, 2010, **114**, 9720–9730.
25 K. M. Eblagon and S. C. E. Tsang, *Appl. Catal., B*, 2014, **160**, 22–34.
26 K. M. Eblagon and S. C. E. Tsang, *Appl. Catal., B*, 2015, **163**, 599–610.
27 Y. Wu, H. Yu, Y. Guo, Y. Zhang, X. Jiang, B. Sun, K. Fu, J. Chen, Y. Qi, J. Zheng and X. Li, *J. Mater. Chem. A*, 2019, **7**, 16677–16684.
28 C. Wan, Y. An, G. Xu and W. Kong, *Int. J. Hydrogen Energy*, 2012, **37**, 13092–13096.
29 H. Mizoguchi, M. Okunaka, M. Kitano, S. Matsuishi, T. Yokoyama and H. Hosono, *Inorg. Chem.*, 2016, **55**, 8833–8838.
30 M. Kitano, S. Kanbara, Y. Inoue, N. Kuganathan, P. V. Sushko, T. Yokoyama, M. Hara and H. Hosono, *Nat. Commun.*, 2015, **6**, 1–9.
31 F. Hayashi, Y. Toda, Y. Kanie, M. Kitano, Y. Inoue, T. Yokoyama, M. Hara and H. Hosono, *Chem. Sci.*, 2013, **4**, 3124–3130.
32 V. K. Fedotov, V. E. Antonov, I. O. Bashkin, T. Hansen and I. Natkaniec, *J. Phys.: Condens. Matter*, 2006, **18**, 1593–1599.
33 M. Oetzel and G. Heger, *J. Appl. Crystallogr.*, 1999, **32**, 799–807.
34 A. Fujimori and L. Schlapbach, *J. Phys. C: Solid State Phys.*, 1984, **17**, 341–351.
35 T. Mongstad, A. Thogersen, A. Subrahmanyam and S. Karazhanov, *Sol. Energy Mater. Sol. Cells*, 2014, **128**, 270–274.
36 D. Zhu, H. Jiang, L. Zhang, X. Zheng, H. Fu, M. Yuan, H. Chen and R. Li, *ChemCatChem*, 2014, **6**, 2954–2960.
37 F. Wu, Y. An, L. Song, G. Xu and L. Xia, *Chem. React. Eng. Technol.*, 2015, **31**, 407–411.
38 X. Ye, Y. An and G. Xu, *J. Alloys Compd.*, 2011, **509**, 152–156.
39 D. Forberg, T. Schwob, M. Zaheer, M. Friedrich, N. Miyajima and R. Kempe, *Nat. Commun.*, 2016, **7**, 1–6.
40 J. Wang, K. Fu, X. Li and G. Li, *Vacuum*, 2019, **162**, 67–71.
41 J. Wang, G. Li, K. Fu and X. Li, *J. Mater. Sci.*, 2019, **54**, 13334–13343.
42 K. Fu, X. Jiang, Y. Guo, S. Li, J. Zheng, W. Tian and X. Li, *Prog. Nat. Sci.: Mater. Int.*, 2018, **28**, 332–336.